PERGAMON

International Journal of Heat and Mass Transfer 43 (2000) 2669–2680

International Journal of HEAT and MASS TRANSFER

www.elsevier.com/locate/ijhmt

Slip-flow heat transfer in circular tubes

Francisco Ezquerra Larrodé[a], Christos Housiadas[b,*], Yannis Drossinos[a]

[a]European Commission, Joint Research Centre, I-21020 Ispra VA, Italy
[b]National Centre for Scientific Research "Demokritos", P.O. Box 60228, GR-15310 Agia Paraskevi, Athens, Greece

Received 18 January 1999; received in revised form 25 October 1999

Abstract

The influence of rarefaction on heat transfer in circular tubes is studied. A spatial rescaling factor ρ_s, which is a measure of rarefaction through its dependence on the Knudsen number, is introduced to identify similarities with the classical Graetz problem. It is found that heat transfer depends both on the degree of rarefaction and on the surface accommodation coefficients. The temperature jump at the wall, ignored in recent investigations, is found to be of essential importance in the heat transfer analysis. A novel uniform asymptotic approximation to high-order eigenfunctions is derived that allows an efficient and accurate determination of the region close to the entrance. © 2000 Elsevier Science Ltd. All rights reserved.

Keywords: Extended Graetz problem; Slip flow; Knudsen number; Rarefaction; Langer transformation; Uniform asymptotic approximation

1. Introduction

Flows for which rarefaction effects start to become non-negligible — the molecular structure of the fluid can no longer be ignored — are in the slip-flow regime [1]. Such flows are characterized by a finite, but small, Knudsen number Kn defined as the ratio of the molecular mean free path λ to the characteristic length of the system, $2R$ for laminar pipe flows. Continuum equations apply for $Kn \to 0$, while kinetic theory is valid for $Kn \to \infty$ (free molecular flow). Slip-flow effects are important in exchange processes in rarefied gases (low-pressure systems) [2] and in microscale heat transfer (ordinary pressures) [3].

An important problem in rarefied gas dynamics is the determination of an adequate set of equations that describes the behaviour at intermediate values of the Knudsen number. In the slip-flow regime, departure from continuum behaviour is slight, corresponding to Knudsen numbers in the range of 10^{-3}–10^{-1} [1]. Such a deviation from continuum behaviour arises first from the walls, where in a non-negligible Knudsen layer [4] molecular collisions with the walls dominate over intermolecular collisions. Far from this layer intermolecular collisions are dominant. Hence, it is intuitive to model flow and heat transfer phenomena in slip flows by maintaining the usual continuum equations for the bulk of the fluid (Navier–Stokes, Fourier heat conduction law) relegating rarefaction effects to the boundary conditions for the temperature and velocity fields (thereby incorporating wall effects) [1,5].

Convective heat transfer under slip-flow conditions in circular tubes was recently analyzed by Barron and co-workers [6,7] by considering it as an extended Graetz problem. As is well known the *côrps* of the

* Corresponding author.
E-mail address: christos@ipta.demokritos.gr (C. Housiadas).

0017-9310/00/$ - see front matter © 2000 Elsevier Science Ltd. All rights reserved.
PII: S0017-9310(99)00324-5

Nomenclature

C_n	coefficient defined in Eq. (20)
c_1, c_2	integration constants given by Eqs. (35) and (36), respectively
c_p	specific heat
F	eigenfunctions, cf. Eq. (16)
${}_1F_1$	confluent hypergeometric function
F_w	weighted asymptotic expansion, cf. Eq. (39)
G	function defined in Eq. (32)
H	function defined in Eq. (30)
h	heat transfer coefficient
J	Bessel function
k	thermal conductivity
Kn	Knudsen number $[\lambda/(2R)]$
Nu	Nusselt number $(2Rh/k)$
Pr	Prandtl number $(\mu c_p/k)$
q	heat flux to the wall
$\hat{r}$	radial coordinate
r	dimensionless radial coordinate $(\rho_s\hat{r}/R)$
$\mathscr{R}$	gas constant for the gas in question
R	pipe radius
R_n	coefficient defined in Eq. (19)
Re	Reynolds number $(2RU_{ave}\varrho/\mu)$
T	temperature
T_w	wall temperature
T_0	inlet temperature
U	fluid velocity
U_{ave}	fluid flux-average velocity $[U_{ave}/U_{max} = (2-\rho_s^2)/2]$
U_{max}	fluid maximum velocity (at the tube centreline, $\hat{r}=0$)
u	dimensionless fluid velocity (U/U_{max})
$\hat{z}$	axial coordinate
z	dimensionless axial coordinate $[\hat{z}\rho_s^2(2-\rho_s^2)/(RRePr)]$
z^+	dimensionless axial coordinate $[\hat{z}/(RRePr)]$

Greek symbols

α_M	tangential momentum accommodation coefficient
α_T	thermal accommodation coefficient
β_v	defined in Eq. (3)
β_T	defined in Eq. (4)
β	β_T/β_v
γ	ratio of specific heats
θ	dimensionless temperature $[(T-T_w)/(T_0-T_w)]$
θ_m	dimensionless bulk-average temperature
λ	mean free path, eigenvalue
μ	fluid viscosity
ρ_s	slip radius, cf. Eq. (6)
ϱ	fluid density

classical Graetz problem is steady-state heat transfer in laminar duct flow under the assumptions of constant-properties fluid, fully developed velocity profile, and negligible energy dissipation. Whereas an analytical solution in terms of an infinite series for the classical Graetz problem exists, the numerical evaluation of high-order eigenvalues and eigenfunctions (required for the determination of the region close to the entrance) is computationally intensive. In fact, the results presented in Refs. [6,7] demonstrate the difficulty of the numerical evaluation of *Kn*-dependent eigenvalues. Mikhailov and Cotta [8] correctly pointed out that the numerical procedure used in these references ignored recent techniques that would have rendered the calculation free of numerical instabilities. More importantly, in Refs. [6,7], the temperature jump condition, although explicitly mentioned in the specification of the boundary conditions, was ignored in the calculation of the eigenvalues. Hence, the heat transfer results of Refs. [6,7] neglect in reality the effect of the temperature jump at the wall, a boundary condition that, as we will show, is crucial in determining heat transfer.

The objective of the present work is to investigate slip-flow heat transfer when both the velocity slip and the temperature jump condition are taken into account. We will show that heat transfer depends on the degree of rarefaction and on gas-surface interaction properties, as determined by the corresponding accommodation coefficients. In doing so we reconsider the slip-flow heat transfer problem by analogy to the classical Graetz problem. We show that a judicious scaling of the spatial variables maps it to the classical Graetz problem with mixed boundary condition. The scaling factor incorporates both rarefaction effects and gas-surface interaction properties: different degrees of rarefaction or gas-surface interaction parameters lead to shifts in the radial position where the wall boundary condition is applied. We find that heat transfer decreases when the temperature jump condition is incorporated, thus, neglecting it leads to significant overprediction of heat transfer. Moreover, these parametric effects are enhanced in the entrance region requiring asymptotic evaluations of eigenvalues and eigenfunctions. Finally, our results are extensively compared to those of Ref. [7].

Our analysis of heat transfer in the entrance region, where high-order eigenvalues are required, lead us to the development of an improved asymptotic analysis of the eigenfunctions. Specifically, the well known asymptotic approximation of Sellars et al. [9] is replaced by a new uniform approximation that incorporates naturally this moving (as rarefaction varies) boundary condition. This novel asymptotic analysis is based on the use of the Langer transformation [10] at two turning points and the subsequent matching of two asymptotic series by appropriately weighting them, thereby obtaining a weighted asymptotic approximation to the high-order eigenfunctions. In the limit of continuum flow, this new approximation improves the accuracy of the original asymptotic approximation reported in Ref. [9] (see also Ref. [11]).

2. The Graetz problem under slip-flow conditions

When the Knudsen number is small but non-negligible the continuum momentum and energy equations are assumed to be valid and slip-flow effects are incorporated by imposing appropriate boundary conditions [1,5]. In particular, the boundary conditions become

$$U(R) = -\beta_v \lambda \frac{dU}{d\hat{r}}|_{\hat{r}=R} + 3\left(\frac{\mathscr{R}T}{8\pi}\right)^{1/2} \frac{\lambda}{T}\frac{\partial T}{\partial \hat{z}}|_{\hat{r}=R}, \quad (1)$$

$$T(R) - T_w = -\beta_T \lambda \frac{\partial T}{\partial r}|_{\hat{r}=R} + \frac{1}{4\mathscr{R}} U^2(R). \quad (2)$$

The derivation of the velocity boundary condition is reproduced in, for example, Refs. [1,4], whereas extensive discussions of the temperature condition may be found in Refs. [2,12]. The first terms on the right-hand side of Eqs. (1) and (2) specify the velocity slip and temperature jump due to a velocity and temperature gradient, respectively. The second term in Eq. (1) accounts for thermal creep, i.e., fluid flow along the wall due to a temperature gradient across the flow, while the second term in Eq. (2) accounts for viscous heat dissipation. The relative importance of these second terms may be shown to be negligible under the usual assumption of low Eckert number (negligible energy dissipation). Indeed, one may readily show via dimensional analysis that the second term in Eq. (1) becomes second order in the Knudsen number, while the second term in Eq. (2) becomes proportional to the Eckert number. Hence, hereafter, only the first terms of the boundary conditions will be retained.

The coefficients β_v and β_T depend on properties of the interaction of the gas with the surface: they are functions of surface accommodation coefficients. Expressions for them may be derived from kinetic-theory arguments (see, for example, Refs. [1,4]). In particular, they are

$$\beta_v = \frac{2-\alpha_M}{\alpha_M}, \quad (3)$$

$$\beta_T = \frac{2-\alpha_T}{\alpha_T}\frac{2\gamma}{\gamma+1}\frac{1}{Pr}. \quad (4)$$

A tangential momentum accommodation coefficient $\alpha_M = 0$ corresponds to specular reflection, whereas $\alpha_M = 1$ corresponds to perfect accommodation (diffuse scattering); in typical engineering applications α_M is close to unity. The thermal accommodation coefficient α_T is close to 0.9 for typical engineering surfaces, but it may become of the order of 10^{-1} for especially clean surfaces [1,5]. In general, tabulated data imply that the accommodation coefficients may be significantly different from unity for light atoms (helium) whereas they are closer to unity for heavy atoms (krypton). Moreover, diffuse scattering becomes dominant for contaminated surfaces with respect to clean surfaces (i.e., $\alpha_M \to 1$) [2].

The velocity-slip condition modifies the Hagen–Poiseuille velocity profile; the resulting profile, expressed in terms of the dimensionless variable $\hat{r}/R$, becomes

$$u\left(\frac{\hat{r}}{R}\right) = \frac{U}{U_{max}} = \frac{1-(\hat{r}/R)^2+4\beta_v Kn}{1+4\beta_v Kn}. \quad (5)$$

Eq. (5) may be further simplified by introducing a new dimensionless radius $r = \rho_s \hat{r}/R$ where the scaling factor ρ_s, hereafter referred to as *slip radius*, is given by

$$\rho_s^2 = \frac{1}{1+4\beta_v Kn}. \quad (6)$$

With this spatial scaling, the dimensionless velocity profile takes the standard parabolic form, $u(r) = 1 - r^2$. An interpretation of the slip radius stems from the observation that ρ_s is the necessary scaling (to first order in the Knudsen number) of the physical boundary at R to a new fictitious extrapolated boundary at R/ρ_s where the fluid velocity does not slip, $U(R/\rho_s) = 0$. In particular, since $\sqrt{1+4\beta_v Kn} \approx 1 + 2\beta_v Kn$ for $\beta_v Kn \ll 1$, the ratio R/ρ_s becomes $R/\rho_s \approx R + \beta_v \lambda$. Then, the condition that the velocity vanish at the extrapolated boundary corresponds to the naive resummation of the velocity boundary condition (1) (keeping, as argued before, only the velocity-slip term). Note that the extrapolated boundary is such that $R/\rho_s > R$ since $\rho_s < 1$. Clearly, the slip radius becomes unity in continuum flows. Henceforth, all quantities will be expressed in terms of ρ_s, for this incorporates both rarefaction effects and gas–surface interaction properties.

We now consider heat transfer in forced laminar flow through a circular tube with constant temperature at the wall with the usual assumptions of the classical Graetz problem: hydrodynamically fully developed flow, constant-properties fluid, high Peclet number, and negligible energy dissipation. The dimensionless energy equation reads

$$(1-r^2)\frac{\partial\theta}{\partial z}=\frac{1}{r}\frac{\partial}{\partial r}\left(r\frac{\partial\theta}{\partial r}\right), \tag{7}$$

with boundary conditions

$$\theta(r,0)=1, \tag{8}$$

$$\frac{\partial\theta}{\partial r}|_{r=0}=0, \tag{9}$$

$$\theta(\rho_s,z)+\frac{\beta}{2}\frac{1-\rho_s^2}{\rho_s}\frac{\partial\theta}{\partial r}|_{r=\rho_s}=0, \tag{10}$$

where the dimensionless variables are defined as follows

$$r=\frac{\hat{r}}{R}\rho_s,\quad z=\frac{\hat{z}}{R}\frac{\rho_s^2(2-\rho_s^2)}{RePr},\quad \theta=\frac{T-T_w}{T_0-T_w}. \tag{11}$$

In the limit of continuum flow ($Kn\to 0$, $\rho_s\to 1$) the usual dimensionless variables are recovered [11].

Thus, the slip-flow Graetz problem has been reduced to a classical Graetz problem with a mixed boundary condition (10). Such cases have been investigated extensively in the literature (see, for example, Ref. [13] and references therein). Therefore, previous results may be easily transposed to the slip-flow problem. A review of the solution of Eq. (7) is instructive because the mixed boundary condition introduces the slip radius explicitly.

As is well known, the infinite series solution of Eq. (7) is

$$\theta(r,z)=\sum_{n=1}^{\infty}a_n\exp\left(-\lambda_n^2 z\right)F(r;\lambda_n), \tag{12}$$

where the eigenfunctions $F(r;\lambda_n)$ satisfy

$$\frac{d^2F}{dr^2}+\frac{1}{r}\frac{dF}{dr}+\lambda^2(1-r^2)F=0, \tag{13}$$

subject to the boundary conditions

$$\frac{dF}{dr}|_{r=0}=0, \tag{14}$$

$$F(\rho_s)+\frac{\beta}{2}\frac{1-\rho_s^2}{\rho_s}\frac{dF}{dr}|_{r=\rho_s}=0. \tag{15}$$

The eigenfunctions F are determined up to a constant due to the linearity of Eq. (13) and the homogeneous boundary conditions. We chose the same normalization $F(0)=1$ as used for the classical Graetz problem.

The eigenfunctions may be expressed in terms of the confluent hypergeometric function [14] (or, alternatively, in terms of Whittaker functions [15]) as follows

$$F(r;\lambda)=\exp\left(-\frac{\lambda r^2}{2}\right){}_1F_1\left[\frac{2-\lambda}{4};1;\lambda r^2\right]. \tag{16}$$

Moreover, the eigenfunctions satisfy orthogonality conditions, since the corresponding differential equation and boundary conditions constitute a Sturm–Liouville problem. The orthogonality condition is given below, along with another useful integral relationship which will be required later

$$\int_0^{\rho_s} r(1-r^2)F(r;\lambda_n)F(r;\lambda_m)\,dr = \begin{cases}0 & \text{for } n\neq m\\ C_nR_n/(4\lambda_n) & \text{for } n=m\end{cases}, \tag{17}$$

$$\int_0^{\rho_s} r(1-r^2)F(r;\lambda_n)\,dr=-\frac{\rho_s}{\lambda_n^2}R_n, \tag{18}$$

where the coefficients R_n and C_n are defined by

$$R_n=\left(\frac{\partial F}{\partial r}\right)_{\substack{r=\rho_s\\ \lambda=\lambda_n}}, \tag{19}$$

$$C_n=2\rho_s\left(\frac{\partial F}{\partial\lambda}\right)_{\substack{r=\rho_s\\ \lambda=\lambda_n}}+\beta(1-\rho_s^2)\left(\frac{\partial^2F}{\partial r\partial\lambda}\right)_{\substack{r=\rho_s\\ \lambda=\lambda_n}}. \tag{20}$$

The eigenvalues λ_n are the roots of the transcendental equation that arises from boundary condition (15), namely

$$\begin{aligned}&{}_1F_1\left(\frac{2-\lambda}{4};1;\lambda\rho_s^2\right)\\ &\quad+\frac{\beta}{2}\lambda(1-\rho_s^2)\left[\frac{2-\lambda}{2}{}_1F_1\left(\frac{6-\lambda}{4};2;\lambda\rho_s^2\right)\right.\\ &\quad\left.-{}_1F_1\left(\frac{2-\lambda}{4};1;\lambda\rho_s^2\right)\right]=0.\end{aligned} \tag{21}$$

The constants a_n are determined from Eq. (8) by invoking the orthogonality properties of the eigenfunctions. Consequently, the local temperature field is

$$\theta(r,z)=-4\rho_s\sum_{n=1}^{\infty}\frac{\exp\left(-\lambda_n^2 z\right)F(r;\lambda_n)}{C_n\lambda_n}, \tag{22}$$

and the mean temperature (flux-averaged), which with the present dimensionless variables reads

$$\theta_m(z) = \frac{4}{\rho_s^2(2-\rho_s^2)} \int_0^{\rho_s} \theta(r,z)(1-r^2) r \, dr, \tag{23}$$

is given by

$$\theta_m(z) = \frac{16}{2-\rho_s^2} \sum_{n=1}^{\infty} \frac{R_n \exp\left(-\lambda_n^2 z\right)}{C_n \lambda_n^3}. \tag{24}$$

It is easy to verify that when $\rho_s \to 1$ the solution of the classical Graetz problem is recovered. The calculation of the Nusselt number requires consideration of the work done by the sliding friction since the total heat flux to the wall is [16]

$$q = -k \frac{\partial T}{\partial \hat{r}}|_{\hat{r}=R} - \mu U(R) \frac{\partial U}{\partial \hat{r}}|_{\hat{r}=R}. \tag{25}$$

As in the case of the temperature boundary condition (2) the second term may be neglected for low Eckert numbers. Thus, the local Nusselt number can be written as

$$Nu = -\frac{2\rho_s}{\theta_m} \frac{\partial \theta}{\partial r}|_{r=\rho_s}, \tag{26}$$

which upon inserting Eqs. (22) and (24) becomes

$$Nu = \frac{\rho_s^2(2-\rho_s^2)}{2} \frac{\sum_{n=1}^{\infty} R_n \exp\left(-\lambda_n^2 z\right)/(C_n \lambda_n)}{\sum_{n=1}^{\infty} R_n \exp\left(-\lambda_n^2 z\right)/\left(C_n \lambda_n^3\right)}. \tag{27}$$

In addition, the fully developed Nusselt number attains the value

$$Nu_\infty = \frac{\rho_s^2(2-\rho_s^2)}{2} \lambda_1^2(\rho_s;\beta). \tag{28}$$

Naive inspection of Eq. (28) suggests that the Nusselt number decreases with decreasing ρ_s, i.e., with increasing rarefaction. Note, however, that this trend is not necessarily true because the eigenvalues depend on parameters ρ_s and β, as can be seen from Eq. (21). For clarity we have explicitly indicated this dependence in Eq. (28). As shown below, with increasing rarefaction the Nusselt number may increase, decrease, or even remain unchanged, depending on the value of β. This important feature is discussed in detail in Section 4.

The numerical evaluation of the mean temperature (series (24)) and of the local Nusselt number (series (27)) requires values for the eigenvalues λ_n and the constants R_n, C_n. The calculation of the local temperature field (series (22)) depends explicitly, in addition, on the eigenfunctions. The eigenvalues can be calculated from Eq. (21) with any standard root-finding method. With the eigenvalues known, the eigenfunctions are then determined from Eq. (16), and subsequently the constants R_n and C_n are obtained by evaluating numerically the integrals (17) and (18). All the aforementioned calculations may be easily performed for low orders with any high-accuracy numerical program like *Mathematica* [17] (see, for example, Ref. [8]). However, for high orders (required to determine the region close to the entrance) computing time becomes prohibitively long. An alternative way is to use asymptotic values for the high-order eigenvalues, eigenfunctions and constants [9,11], a subject that is discussed in the next section.

3. Uniform asymptotic approximation

A first-order asymptotic approximation to the solution of Eq. (13) was initially derived by Sellars et al. in Ref. [9]. Their asymptotic approximation to the high-order eigenfunctions consisted in the so-called WKB approximation (named after Wentzel, Kramers, and Brillouin, see, for instance, Ref. [18]), which however is valid only for intermediate r because it becomes singular at $r = 0$ (regular singular point of Eq. (13)) and at $r = 1$ (turning point of Eq. (13)). The usual way to handle these singularities is to provide in addition to the WKB approximation (denoted by F_B), two approximations to the exact solution valid for r near the centreline (F_A) and for r near the wall (F_C), as well as two matching functions F_{AB} and F_{BC}, which match appropriately the two solutions F_A and F_C to the WKB approximation F_B. Accordingly, a uniform WKB approximation over the whole interval $0 \le r \le 1$ is obtained as $F_{WKBU} = F_A + F_B + F_C - F_{AB} - F_{BC}$. This approach was used in Ref. [11] where explicit expressions for all these functions may be found.

For the classical Graetz problem the eigenvalues are obtained by solving equation $F = 0$ at $r = 1$. Hence, it is sufficient to require $F_C = 0$, a condition that greatly simplifies the analysis. In the case of slip flow boundary condition, Eq. (15) must be imposed at $r = \rho_s \le 1$. According to Ref. [9] the approximate form F_C is valid for $\lambda_n^{2/3}(1-r) \ll 1$; thus, for a given r there exists a value of n such that the approximation ceases to be valid. Therefore, the complete function F_{WKBU} should be used in Eq. (15). Unfortunately, this procedure, although sound, leads to very cumbersome and complicated calculations since boundary condition (15) involves the derivative of the eigenfunction.

Alternatively, we considered a different approach to obtain a uniform asymptotic approximation. Specifically, the Langer transformation was used (see, for example, Refs. [10,18]) that, besides providing a uni-

form asymptotic approximation over a region including the turning point $r = 1$, gave more accurate results than the uniform WKB approximation. The algebraic manipulations required to obtain the uniform Langer approximation at $r = 1$ are reproduced in Appendix A.1 The resulting asymptotic approximation, denoted by F_1, is

$$F_1(r) = \frac{H(r)^{1/2}}{r^{1/2}(1-r^2)^{1/4}}\left[c_1 J_{1/3}(\lambda H) + c_2 J_{-1/3}(\lambda H)\right], \quad (29)$$

where

$$H(r) = \int_r^1 \mathrm{d}s(1-s^2)^{1/2} = \frac{1}{2}\left[\arccos r - r(1-r^2)^{1/2}\right]. \quad (30)$$

The function F_1 is a valid asymptotic approximation for $r \gg 1/\lambda$, becoming singular at $r = 0$. Thus, another approximation, valid in the region close to $r = 0$, is required. We show in Appendix A.2 that a suitable change of variables allows the use of the same scheme to determine an asymptotic approximation valid in a region that includes $r = 0$. This approximation, denoted by F_0, is

$$F_0(r) = c_0 \frac{G(r)^{1/2}}{r^{1/2}(1-r^2)^{1/4}} J_0(\lambda G), \quad (31)$$

where

$$G(r) = \frac{\pi}{4} - H(r). \quad (32)$$

This is a valid approximation for $r \ll 1 - 1/\lambda^{2/3}$. Since Eq. (13) is linear, all constant multiples of a solution are also solutions. Hence, the integration constant c_0 is merely a scaling factor which can be chosen arbitrarily. As discussed in Section 2 $c_0 = 1$ so that $F_0(0) = 1$, as scaled in the original Graetz solution [9]. The constants c_1 and c_2 will be determined by the standard method of asymptotic matching [18]: specifically, since the two asymptotic approximations share a common interval of validity, $1/\lambda \ll r \ll 1 - 1/\lambda^{2/3}$, we require that both functions be asymptotically equal on that interval as $\lambda \to \infty$. The behaviour of F_0 and F_1 for large values of their arguments can be determined from the asymptotic expansions of the appropriate Bessel functions (as reproduced, for example, in Ref. [10]). One obtains

$$F_0(r) \sim \left(\frac{2}{\lambda\pi r}\right)^{1/2} \frac{\cos(\lambda G - \pi/4)}{(1-r^2)^{1/4}}, \quad (33)$$

$$F_1(r) \sim \left(\frac{2}{\lambda\pi r}\right)^{1/2} \frac{1}{(1-r^2)^{1/4}} \times \left[c_1 \cos\left(\frac{\lambda\pi}{4} - \lambda G - \frac{5\pi}{12}\right) + c_2 \cos\left(\frac{\lambda\pi}{4} - \lambda G - \frac{\pi}{12}\right)\right]. \quad (34)$$

We determine the constants by equating the asymptotic expansions (33) and (34) to obtain

$$c_1 = \frac{2}{\sqrt{3}} \sin\left(\frac{\lambda\pi}{4} - \frac{\pi}{3}\right), \quad (35)$$

$$c_2 = -\frac{2}{\sqrt{3}} \sin\left(\frac{\lambda\pi}{4} - \frac{2\pi}{3}\right). \quad (36)$$

These constants are identical to those reported in Ref. [9] since the asymptotic expressions presented in this section apply equally well to the classical Graetz problem.

3.1. Asymptotic calculation of eigenvalues and related constants

The numerical values of the quantities of interest λ_n, R_n, and C_n are calculated respectively from Eqs. (15), (19) and (20) by substituting for F the asymptotic approximation which is valid in the region close to the wall, namely F_1. The final expressions are obtained after some tedious, but straightforward algebra. They are lengthy combinations of Bessel functions and their derivatives, which nevertheless can be evaluated numerically with ease. For reference purposes, we only present the equation that gives the asymptotic eigenvalues

$$\left(1-\rho_s^2\right)\sqrt[5/4]{\frac{H(\rho_s)}{\rho_s}} \times \left\{c_1\left(\frac{\beta\lambda}{4\rho_s}\left[J_{4/3}(\lambda H) - J_{-2/3}(\lambda H)\right] + \left[\frac{1}{\left(1-\rho_s^2\right)^{3/2}} - \frac{\beta C}{4\rho_s}\right] J_{1/3}(H)\right) + c_2\left(\frac{\beta\lambda}{4\rho_s}\left[J_{2/3}(\lambda H) - J_{-4/3}(\lambda H)\right] + \left[\frac{1}{\left(1-\rho_s^2\right)^{3/2}} - \frac{\beta C}{4\rho_s}\right] J_{-1/3}(\lambda H)\right)\right\} = 0, \quad (37)$$

where

$$C = \frac{1}{H(\rho_s)} + \frac{1-2\rho_s^2}{\rho_s\left(1-\rho_s^2\right)^{3/2}}. \quad (38)$$

Note that the eigenvalues become smooth functions of Kn, reproducing the well-known asymptotic eigenvalues of the classical case at $Kn = 0$, i.e., $\lambda_1 = 2.667$, $\lambda_2 = 6.667$, etc. Table 1 shows the exact

and asymptotic eigenvalues at orders $n \geq 5$ for $\rho_s = 0.95$ and $\beta = 10$. The exact values were obtained by solving Eq. (21) where *Mathematica* [17] was used to evaluate numerically the confluent hypergeometric function. For comparison purposes various asymptotic approximations are shown in Table 1. In particular, the asymptotic values were calculated by substituting in Eq. (15) (i) the uniform Langer approximation F_1, which leads to Eq. (37) above; (ii) the uniform WKB approximation F_{WKBU}, as used in Ref. [11]; (iii) the approximate form F_{C}, valid close to the wall; and (iv) the WKB approximation F_{B}, valid for intermediate r. It is apparent that the uniform approximations (i) and (ii) give excellent results.

3.2. Weighting the Langer approximations

The two approximate eigenfunctions F_0 and F_1 fail to cover the whole interval of interest because they become singular at $r = 1$ and $r = 0$, respectively. The usual method of asymptotic matching (used to determine the coefficients c_1 and c_2) can not be used to obtain a uniform asymptotic expression since the two functions themselves are asymptotic. The problem, essentially, reduces to combining these functions in a way to cancel the respective divergent parts at the boundaries of the interval. We propose to combine them by choosing a suitable weight, thereby obtaining a weighted asymptotic approximation as follows

$$F_{\mathrm{w}}(r) = w_0(r)F_0(r) + w_1(r)F_1(r), \tag{39}$$

with

$$w_0(r) + w_1(r) = 1. \tag{40}$$

The weighting functions w_0 and w_1 are to be chosen such that each function is enhanced in its region of validity and it is reduced close (or at) the point where the function becomes singular. Hence, the singular behaviour of either functions at the boundary

$$F_0(r) \sim O\left[(1-r)^{-1/4}\right], \quad \text{as } r \to 1, \tag{41}$$

$$F_1(r) \sim O(r^{-1/2}), \quad \text{as } r \to 0, \tag{42}$$

provides a lower bound on the behaviour of the weighting functions. The weights were determined numerically by minimizing the difference of the weighted asymptotic approximation to the exact as computed with *Mathematica* [17]. The error was defined as the Euclidean (L_2) norm of the difference between the two functions (see, for example, Ref. [11]). For simplicity we tried weights of the form $W = (1 - r^a)^b$ which for $r \to 1$ behaves as $O[(1-r)^b]$, while $1 - W$ behaves as $O[r^a]$ when $r \to 0$. The best combination we found numerically was

$$w_0(r) = (1 - r^2)^2, \tag{43}$$

$$w_1(r) = r^2(2 - r^2). \tag{44}$$

The numerical procedure used to specify the exponents a and b corresponds to a numerical minimization of the difference of two functions, namely a global minimization. An alternative way to specify them is to impose constraints on the derivative of F_{w} at the two end points, namely a local requirement. We found the two approaches gave slightly different values, the global minimization being preferable.

The absolute difference between the weighted asymptotic approximation and the exact solution is shown in Fig. 1 as function of r for order $n = 5$ and $\rho_s = 1$ (dashed curve). For comparison with our previous work we also show the corresponding difference of the uniform WKB approximation (F_{WKBU}) as presented in Ref. [11] (solid curve). The error of the weighted asymptotic expansion is significantly reduced with respect to the uniform WKB approximation, and more importantly, it is uniform over the whole interval. This improvement justifies the development of a new asymptotic approximation to the eigenfunctions of Eq. (13).

4. Results

The local Nusselt number, being the primary quantity of interest in heat transfer calculations, was determined as a function of axial distance. The required input parameters are the product $\beta_{\mathrm{v}} Kn$ (or, equiv-

Table 1
Asymptotic eigenvalues at $\rho_s = 0.95$ and $\beta = 10$

Order	Exact	Uniform Langer (F_1)	F_{C}	F_{B}	Uniform WKB (F_{WKBU})
5	17.6707	17.6683	17.7540	18.3051	17.6722
6	21.6824	21.6803	21.7570	22.2338	21.6851
7	25.7026	25.7007	25.7703	26.1841	25.7058
8	29.7287	29.7270	29.7909	30.1519	29.7322

alently, the slip radius ρ_s) which is a measure of rarefaction, and the ratio $\beta = \beta_T/\beta_v$ which is a function of accommodation coefficients, i.e., a property of gas–surface interactions. The parameter $\beta_v Kn$ was considered to vary between zero (continuum regime) and 0.1: this range corresponds to $1 \geq \rho_s \geq 0.845$. On the other hand, β was considered to vary between 0 and 10.

The necessary eigenvalues and constants in Eq. (27) were evaluated as described in Sections 2 and 3. In particular, the infinite series was truncated at $n = 30$: summation of the first 30 terms provided adequate convergence for all $z^+ > 10^{-3}$. The asymptotic approximation developed in Section 3 enabled the determination of the Nusselt number in a reliable manner without experiencing the numerical instabilities reported in Ref. [7]. In the spirit of the approach suggested in Ref. [11], the first four eigenvalues and constants were obtained from an exact evaluation, performed with *Mathematica* [17], whereas orders $5 \leq n \leq 30$ were determined asymptotically.

Fig. 2 shows the effect of parameter $\beta_v Kn$ on the axial evolution of the local Nusselt number. We consider two cases: $\beta = 0$ (Fig. 2(a)) and $\beta = 10$ (Fig. 2(b)). Note that the case $\beta = 0$ is rather artificial, because it requires either $\alpha_T = 2$ or $\alpha_M = 0$ (see Eqs. (3) and (4)). As discussed in Section 2, such values are either unphysical (physically meaningful values of α_T must be in the range 0 to 1) or not typical of practical engineering applications (for which $\alpha_M \simeq 1$). Nevertheless, the case $\beta = 0$ is a useful limiting case corresponding to the assumption of negligible temperature jump. In contrast, the case $\beta = 10$ corresponds to conditions of large temperature jump at the wall. In Fig. 2(a) we also include the results of Barron et al. [7] that, as previously discussed, were obtained by neglecting the temperature jump (i.e., by imposing the artificial condition $\beta = 0$). Inspection of the figure shows that our results agree with these previous results. Moreover, due to the accurate and reliable asymptotic solution presented in this work our calculations cover a much larger part of the entrance region.

Fig. 2(a) shows that heat transfer increases with increasing Knudsen number in the absence of a temperature jump ($\beta = 0$). Instead, Fig. 2(b) suggests that

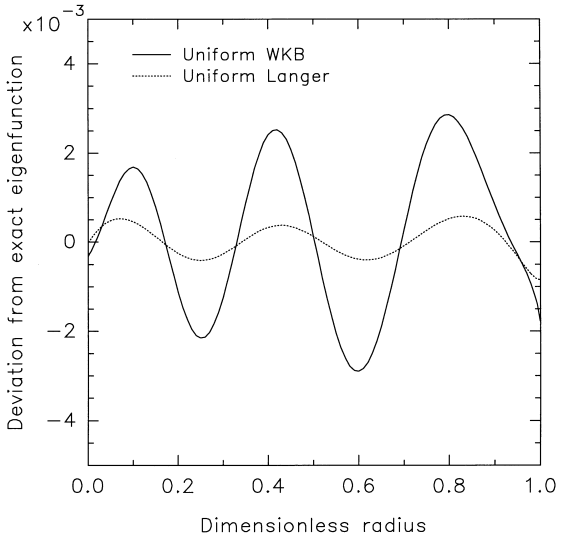

Fig. 1. Absolute deviation of the asympotic eigenfunction from the exact at order $n = 5$.

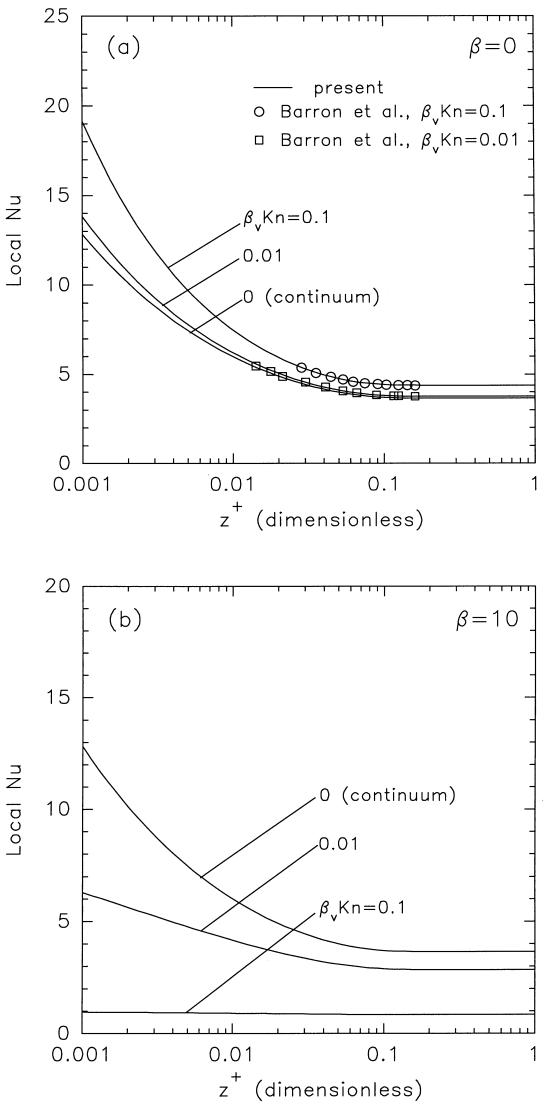

Fig. 2. Local Nusselt number as a function of axial distance and parametrized by $\beta_v Kn$ with no temperature jump, $\beta = 0$ (a), and with large temperature jump $\beta = 10$ (b).

this trend is reversed when a large temperature jump is present. These results may be interpreted by noting that as the flow departs from the continuum regime a reduction in momentum and energy exchange occurs because the corresponding gradients at the surface are smaller due to the velocity slip and the temperature jump [1]. Specifically, when $\beta = 0$ (cf. Fig. 2(a)) the decrease in momentum exchange leads to increased velocity at the wall, thereby increasing convective heat transfer. Hence, as rarefaction increases heat transfer increases. However, when β is large heat transfer is observed to decrease since the temperature gradient at the wall decreases: thus, in this case, heat transfer decreases with increasing rarefaction.

The effect of parameter β, for a fixed value of $\beta_v Kn = 0.1$, is illustrated in Fig. 3. The main observation is that heat transfer in the slip-flow regime decreases with increasing β. As noted earlier, this effect can be attributed to the reduction of energy exchange due to smaller temperature gradients normal to the wall, a consequence of a larger jump at the wall surface. The results of Fig. 3 also show that as β increases, the axial evolution tends to become flatter, hence, the entrance zone is shortened. A consequence of this behaviour is that parametric effects become more pronounced closer to the entrance. The same trend can be observed by inspection of Fig. 2. Thence the interest of obtaining reliable asymptotic methods.

The fully-developed Nusselt number as a function of $\beta_v Kn$ and parametrized by β is presented in Fig. 4. For completeness the results of Ref. [7] are also plotted. This figure illustrates in a compact way the effect of rarefaction on heat transfer: it demonstrates that heat transfer depends not only on the degree of rarefaction but also on β. Specifically, heat transfer decreases with increasing β irrespective of Kn. As rarefaction increases, heat transfer may increase, decrease, or, remain unchanged depending on the value of β.

In Appendix B a perturbative calculation of the eigenvalues shows that for very small Knudsen numbers the first-order correction to them, and hence to Nu_∞ (cf. Eq. (28)), is positive when $\beta < 1$ and negative when $\beta > 1$. Consequently, the following simple criterion may be inferred: in slip flow, heat transfer increases with respect to the continuum regime if $\beta < 1$ and decreases if $\beta > 1$. This is effectively observed in the left part of Fig. 4, where the line corresponding to $\beta = 1$ coincides with the line (dashed) for the fully developed Nusselt number in the continuum regime ($Nu = 3.657$). For larger Kn values the two lines deviate. As can be seen in Fig. 4 the previous criterion on increased (or decreased) heat transfer is quite accurate for $\beta_v Kn < 0.04$ (or $\rho_s > 0.96$). Beyond this range the criterion should be viewed as approximate. Finally, the results presented in Fig. 4 show that the conclusion of Ref. [7] that slip flow is always accompanied by a heat transfer enhancement is not as general as the authors claim, in particular it fails for $\beta > 1$. Note that most engineering applications are concerned precisely with $\beta > 1$.

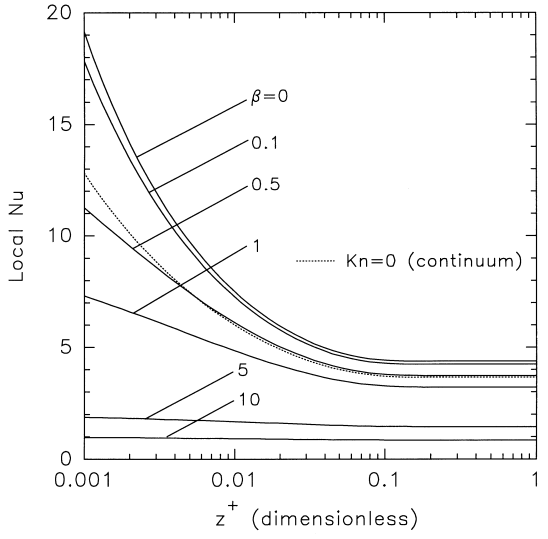

Fig. 3. The effect of parameter β on the axial evolution of the local Nusselt number at $\beta_v Kn = 0.1\,(\rho_s = 0.845)$.

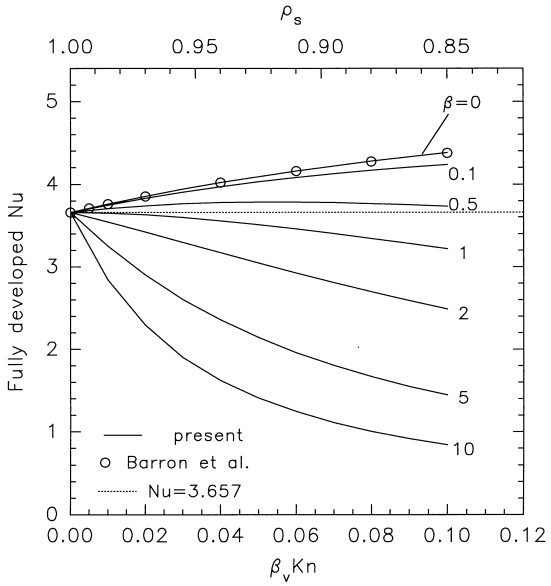

Fig. 4. Fully developed Nusselt number as a function of $\beta_v Kn$ (equivalent ρ_s) and β.

5. Conclusions

Slip-flow heat transfer in circular tubes was studied under conditions that allowed us to exploit its similarities to the classical Graetz problem. We showed that heat transfer depends on two parameters: the product $\beta_v Kn$ (or, alternatively, the slip radius ρ_s) which is a measure of the degree of rarefaction, and β which is a function of the surface accommodation coefficients. The effect of the temperature jump at the wall was determined to be essential in the heat transfer analysis. Our finding agrees with previous results on increased heat transfer when the temperature jump at the wall is neglected ($\beta = 0$), but it also shows the limitations of such a conclusion. In particular, heat transfer was found to increase or decrease with increasing rarefaction depending on whether $\beta < 1$ or $\beta > 1$, respectively. On the other hand, for a given Kn (fixed degree of rarefaction) heat transfer decreases with increasing β. The results were interpreted by noting that under slip-flow conditions gradients at the wall are smaller than in continuum flow due to the velocity slip and the temperature jump.

Moreover, we developed a new uniform asymptotic approximation to the eigenfunctions of the Graetz problem, a weighted asymptotic approximation, that gave improved results with respect to the well-known WKB approximation. The asymptotic expressions were used to determine the heat transfer close to the entrance, a region where rarefaction effects were found to be more pronounced.

Acknowledgements

We would like to thank Peter Hähner for insightful comments on the weighted asymptotic approximation. F.E.L. acknowledges a European Commission Fellowship of the Joint Research Centre.

Appendix A. The Langer transformation applied to the Graetz problem

The WKB approximation fails to provide a suitable approximation in regions close to turning points; this is the reason that the WKB approximation is asymptotically matched with approximate solutions near the turning points. In 1935 Langer showed that with a slight (but significant) modification of the WKB approximation it was possible to obtain a uniform asymptotic approximation valid even in regions containing a turning point [18]. The method is straightforward for single turning points, but for differential equations with more than one turning point the solution of the transformed equation (via the so-called Langer transformation) may be as difficult as the solution of the original equation (see Refs. [10,18,19] and references therein).

Herein, we look for uniform asymptotic approximations to the solution of Eq. (13) valid in the interval $r \in [0, 1]$ for large values of the parameter λ. The WKB approximation will fail at the turning point $r = 1$ and at the regular singular point $r = 0$. By introducing the new independent variable $t = -\log r$ Eq. (13) is transformed into

$$\frac{d^2F(t)}{dt^2} + Q(t)F(t) = 0, \tag{A1}$$

where

$$Q(t) = \lambda^2 e^{-2t}(1 - e^{-2t}). \tag{A2}$$

Thus, through this change of variables both points $t = 0$ (corresponding to $r = 1$), and $t \to \infty$ (corresponding to $r \to 0$) may be treated as turning points since $Q(t)$ is zero at these points. As mentioned earlier, we shall apply the Langer transformation separately to each turning point.

A.1. Langer transformation for $r = 1$ ($t = 0$)

We introduce new dependent and independent variables as follows [10]

$$z = \phi(t), \qquad v(z) = \psi(t)F(t), \tag{A3}$$

where

$$\phi(t) = \left[\frac{3}{2\sqrt{2}}\lambda H(e^{-t})\right]^{2/3}, \qquad \psi(t) = \sqrt{\phi'(t)}. \tag{A4}$$

With this change of variables Eq. (A1) is transformed into

$$\frac{d^2v(z)}{dz^2} + (2z + \delta)v(z) = 0. \tag{A5}$$

The asymptotic approximation consists of solving the previous equation neglecting the δ term: this is a legitimate approximation since z is of order $O[\lambda^{2/3}(1 - r)]$ and δ is of order $O(\lambda^{-4/3})$ for $r \in [0, 1]$ and $\lambda \to \infty$.

Neglecting the δ-term, the solution of Eq. (A5) is

$$v(z) = \sqrt{z}\left[\bar{c}_1 J_{1/3}\left(\frac{2\sqrt{2}}{3}z^{3/2}\right) + \bar{c}_2 J_{-1/3}\left(\frac{2\sqrt{2}}{3}z^{3/2}\right)\right]. \tag{A6}$$

Going back to the original variables, rearranging terms and absorbing the constants into redefined integration constants c_1 and c_2 we obtain Eq. (29).

A.2. Langer transformation for $r = 0$ ($t \to \infty$)

We use the same change of variables as that of Eqs. (A3), but now with

$$\phi(t) = -\log\left[\lambda G(e^{-t})\right], \qquad \psi(t) = \sqrt{\phi'(t)}. \tag{A7}$$

The transformed equation now reads

$$\frac{\mathrm{d}^2 v(z)}{\mathrm{d}z^2} + \left(\mathrm{e}^{-2z} + \delta\right) v(z) = 0. \tag{A8}$$

In this case e^{-2z} is of order $O(\lambda^2 r^2)$ and δ is of order $O(r^2)$. The solution of the approximate equation (neglecting the term δ) is

$$v(z) = \bar{c}_3 J_0(\mathrm{e}^{-z}) + \bar{c}_4 K_0(i\mathrm{e}^{-z}). \tag{A9}$$

The Bessel function K has a logarithmic singularity when its argument tends to zero ($z \to \infty$ or, equivalently, $r \to 0$). Since the function is required to be finite there, we impose $\bar{c}_4 = 0$. As before, returning to the original variables we obtain Eq. (31).

Appendix B. Perturbative calculation of the eigenvalues

Herein, we derive expressions for the eigenvalues in the limiting case $Kn \to 0$, i.e., $1 - \rho_s \ll 1$. The results show explicitly the influence of parameters ρ_s and β on λ_n, and by that on the fully developed Nusselt number, cf. Eq. (28).

In the limit $1 - \rho_s \ll 1$ a uniform first-order expansion of $F(r)$ in Eq. (13) may be performed via the method of strained parameters [10]. Specifically, $F(r)$ and λ are expanded in terms of the small parameter $\xi = 1 - \rho_s$ as follows

$$F(r) = F^{(0)}(r) + \xi F^{(1)}(r) + \cdots \tag{B1}$$

$$\lambda = \lambda^{(0)} + \xi \lambda^{(1)} + \cdots \tag{B2}$$

Since the boundary condition (15) is imposed at $r = 1 - \xi$ it is also expanded about $r = 1$ in a Taylor expansion to obtain the following zeroth-order approximation to Eqs. (13) and (15)

$$\frac{\mathrm{d}^2 F^{(0)}}{\mathrm{d}r^2} + \frac{1}{r}\frac{\mathrm{d}F^{(0)}}{\mathrm{d}r} + \left[\lambda^{(0)}\right]^2 (1 - r^2) F^{(0)} = 0, \tag{B3}$$

$$F^{(0)}(1) = 0. \tag{B4}$$

Eq. (B3) and boundary condition (B4) indicate that, as expected, the zeroth-order eigenfunctions $F_n^{(0)}$ and the eigenvalues $\lambda_n^{(0)}$ are solutions of the case corresponding to $\rho_s = 1$ (classical Graetz problem).

The first-order approximation is given by

$$\frac{\mathrm{d}^2 F^{(1)}}{\mathrm{d}r^2} + \frac{1}{r}\frac{\mathrm{d}F^{(1)}}{\mathrm{d}r} + \left[\lambda^{(0)}\right]^2 (1 - r^2) F^{(1)} = -2\lambda^{(0)}\lambda^{(1)}(1 - r^2) F^{(0)}, \tag{B5}$$

$$F^{(1)}(1) = (1 - \beta)\frac{\mathrm{d}F^{(0)}(1)}{\mathrm{d}r}. \tag{B6}$$

The first-order correction to the eigenvalue, $\lambda^{(1)}$, is obtained by imposing a solvability condition. Specifically, we multiply Eq. (B3) by $F^{(1)}(r)$ and Eq. (B5) by $F^{(0)}(r)$, integrate both from $r = 0$ to $r = 1$, and then we take their difference to obtain an equation that is satisfied only if $\lambda^{(1)}$ is

$$\lambda^{(1)} = \frac{1 - \beta}{2\lambda^{(0)} N_0^2}\left[\frac{\mathrm{d}F^{(0)}(1)}{\mathrm{d}r}\right]^2 \tag{B7}$$

where

$$N_0^2 = \int_0^1 \left[F^{(0)}(r)\right]^2 r(1 - r^2)\,\mathrm{d}r. \tag{B8}$$

Since $\lambda^{(0)}$ is positive the preceding expressions show that the first-order correction is positive for $\beta < 1$ and negative for $\beta > 1$.

References

[1] E.R.G. Eckert, R.M. Drake, Analysis of the Heat and Mass Transfer, McGraw-Hill, New York, 1972.

[2] F. Shapirov, V. Seleznev, Data on internal rarefied gas flows, J. Phys. Chem. Ref. Data 27 (3) (1998) 657–705.

[3] A.B. Duncan, G.P. Peterson, Review of microscale heat transfer, Appl. Mech. Rev 47 (9) (1994) 397–428.

[4] S.A. Schaaf, Mechanics of rarified gases, in: Handbuch der Physik, vol. VIII/2, Springer-Verlag, Berlin, 1963, pp. 591–624.

[5] W.M. Rohsenow, J.P. Hartnett, E.N. Ganić, Handbook of Heat Transfer Fundamentals, 2nd ed., McGraw-Hill, New York, 1985.

[6] R.F. Barron, X. Wang, R.O. Warrington, T. Ameel, Evaluation of the eigenvalues for the Graetz problem in slip-flow, Int. Comm. Heat. Mass Transfer 23 (4) (1996) 563–574.

[7] R.F. Barron, X. Wang, A. Ameel, R.O. Warrington, The Graetz problem extended to slip flow, Int. J. Heat Mass Transfer 40 (8) (1997) 1817–1823.

[8] M.D. Mikhailov, R.M. Cotta, Eigenvalues for the Graetz problem in slip-flow, Int. Comm. Heat and Mass Transfer 24 (3) (1997) 449–451.

[9] J.R. Sellars, M. Tribus, J.S. Klein, Heat transfer to laminar flow in a round tube or flat conduit — the Graetz problem extended, Trans. Am. Soc. Mech. Engrs 78 (1956) 441–448.

[10] A.H. Nayfeh, Introduction to Perturbation Techniques, Wiley, New York, 1981.
[11] C. Housiadas, F. Ezquerra Larrodé, Y. Drossinos, Numerical evalution of the Graetz series, Int. J. Heat and Mass Trasfer 42 (1999) 3013–3017.
[12] G. Rémie, G. Duffa, Corrective term in wall slip equations for Knudsen layer, Journal of Thermophysics 9 (2) (1995) 383–384.
[13] M.D. Mikhailov, M.N. Özisik, Unified Analysis and Solutions of Heat and Mass Diffusion, Wiley, New York, 1984.
[14] H.A. Lauwerier, The use of confluent hypergeometric functions in mathematical physics and the solution of an eigenvalue problem, Appl. Sci. Res., Sect. A 2 (1950) 184–204.
[15] E.T. Whittaker, G.N. Watson, A Course of Modern Analysis, 4th ed., Cambridge University Press, Cambridge, 1927.
[16] S.H. Maslen, On heat transfer in slip flow, Journal of the Aeronautical Science 25 (1958) 400–401.
[17] S. Wolfram, Mathematica: A System for Doing Mathematics by Computer, 2nd ed., Addison-Wesley, Reading, MA, 1991.
[18] C.M. Bender, S.A. Orszag, Advanced Mathematical Methods for Scientist and Engineers, McGraw-Hill, New York, 1978.
[19] F.W.J. Olver, Asymptotics and Special Functions, Computer Science and Applied Mathematics, Academic Press, New York, 1974.